Melt Absorbability of Iron Ore Nuclei and Its Influence on Suitable Liquid Content of Sintered Body

SHENG-LI WU, BO SU, YUAN-HONG QI, MING-YIN KOU, YUAN LI, and WEI-LI ZHANG

Sinter quasi-particles consist of nuclei particles and adhering fines. Therefore, reaction properties of the nuclei ore will ultimately affect the bonding strength of the sintered body. In this study, micro-sintering tests were conducted to explore the melt absorbability of nuclei ore and its effect on the suitable liquid content of the sintered body. The results showed that the melt absorbability is negatively correlated with the lowest assimilation temperature, and the most important mineralogy factor influencing melt absorbability is iron mineral type. The reaction behaviors of melts containing SiO_2 or Al_2O_3 substrates are different, and the reaction process of the melt containing SiO_2 is more complicated. In addition, the bonding strength of the sintered body is collectively determined by the liquid phase fluidity of adhering fines and the assimilability of nuclei ore. The high melt absorbability has an adverse effect on bonding strength, and it requires adhering fines to provide more primary melts to meet the requirements for sintered body bonding strength. In the condition with the same liquid content, for nuclei ore with stronger melt absorbability, an appropriate increase in the adhering fines ratio and reduction in segregation basicity are more conducive to improving the bonding strength.

DOI: 10.1007/s11663-017-1059-9

I. INTRODUCTION

HIGH basicity sinter is one of the major raw materials used in blast furnace ironmaking because its high reducibility and good mechanical strength are significant factors in determining the productivity and efficiency of the blast furnace. However, with the depletion of high-grade iron ores, steel enterprises have to increase the use of low-grade iron ores with high LOI (the loss on ignition) or high gangue content iron ores in the sintering process for economic reasons, which affects the sintering indexes to some extent. With the intention of overcoming the declining quality of iron ore resources, the concept of quasi-particles has been introduced to utilize low-quality iron ore in the sintering process.[1,2]

The quasi-particle consists of coarse ores in the center as nuclei particles and adhering fines of fine ores, flux, and fuel. In the sintering process, the initial melt generates within adhering fines by forming calcium ferrites and silicates with low melting temperatures. Then, the initial melt spreads out and continues to react with the surrounding particles to form the primary melt. Finally, the primary melt reacts with the nucleus, and assimilation occurs to form secondary melts.[3] Therefore, the nuclei ore property plays an important role in affecting the assimilation behavior and sinter qualities of quasi-particles.

Liquid phase formation, wetting and penetration behaviors of different composition adhering fines have been widely investigated,[4–13] but the high-temperature reaction characteristic of iron ore nuclei has rarely been reported. Okazaki *et al.*[14] previously studied the melt evolution process within the adhering layer in quasi-particles using paired tablets consisting of an ore tablet and an initial melt tablet. The morphology of the ore surface before and after dehydration and the chemical composition of ores were found to determine the penetration behavior of the melt, and the product yield and the strength of sinter were reflected by the penetration length of the blended ores. Wu *et al.*[15–17] proposed the new concept of the "melt absorbability characteristic" to estimate the reaction degree between primary melts and nuclei ores, and found that high melt absorbability had an adverse effect on bonding strength. However, the

SHENG-LI WU, MING-YIN KOU, YUAN LI, and WEI-LI ZHANG are with the School of Metallurgical and Ecological Engineering, University of Science and Technology Beijing, Room 503, Yejin Building, No. 30 Xueyuan Road, Haidian District, Beijing 100083, China. BO SU is with the School of Metallurgical and Ecological Engineering, University of Science and Technology Beijing and also with State Key Laboratory of Advanced Steel Processing and Products, Central Iron and Steel Research Institute, Beijing 100081, China. Contact e-mail: ustb_subo@163.com YUAN-HONG QI is with the State Key Laboratory of Advanced Steel Processing and Products, Central Iron and Steel Research Institute.

Manuscript submitted May 19, 2017.
Article published online July 31, 2017.

influential factors and reaction behaviors of the melt absorbability of nuclei ore and its mechanism of impact on bonding strength of the sintered body need to be considered. In addition, as an important direction for optimal design of quasi-particle structures, the effect of the ratio of nuclei to adhering fines on the bonding strength of the sintered body has not been reported.

In the present study, the main influential factors and the reaction behaviors of melts absorbed by nuclei, and the mechanism through which melt absorbability affects the bonding strength of the sintered body, were investigated. The suitable liquid content and the optimized ratio of adhering fines for different melt absorbability nuclei ores were also discussed, which provides theoretical evidence for the analysis of the reaction behavior of primary melts and nuclei particles as well as optimization design of quasi-particle structure.

II. EXPERIMENTAL

A. *Materials Preparation*

Table I shows the chemical composition and major mineral types of iron ores used in the present study. The mineral type was determined by XRD analysis. OA and OB are limonite ores with high crystal water content, OC and OD belonged to Marramanba ores, and OE and OF are hematite with different SiO_2 contents.

B. *Experimental Methods*

1. *Melt absorbability and effective liquid phase fluidity*

The +1 mm size fraction iron ores were crushed into -0.074 mm fines, and then shaped into Φ20 × 6 mm tablets under 60 MPa to simulate nuclei ores. The CaO content of the adhering fines was calculated to be approximately 15 wt pct based on the actual sinter burden constituent.[18] Therefore, in the research, the pre-sintered hematite (crushed into the less than 0.074 mm) added with 15 wt pct content of CaO chemical reagents was prepared to simulate adhering fines. Then, 0.5 g adhering fines were pressed to an 8 mm diameter cylinder tablet under 20 MPa. The experiments were carried out using coupled ore tablets to simulate a quasi-particle structure as shown in Figure 1.

The experimental apparatus and test methods are illustrated in Figure 2. The samples were sintered in an infrared image furnace, simulating an actual sintering temperature and atmosphere system. The sintering temperature was set to 1573 K (1300 °C). Afterwards, the fluidity of the melt formed on the surface of the iron ore substrate was measured with a projection method according to Eq. [1].[17] The samples were then mounted in epoxy resin, dissected perpendicular to the interface, and polished with 1 μm diamond paste. The integrated cross section images of these samples were grained using "Live XY Builder" Modules of a Leica DM4 optical microscope. The penetration depth in the reaction zone was measured at the center and every quarter from the rim to the center (see Figure 2(d)) with an image analysis method, and the melt absorbability of the nuclei ore was expressed as the average of those measurements.

$$\text{Fluidity} = \frac{A_{\text{after}} - A_{\text{before}}}{A_{\text{before}}}, \quad [1]$$

where A_{after} is the vertical projection area after the sintering experiment, mm^2. A_{before} is the vertical projection area before the sintering experiment, mm^2.

2. *Test of the bonding strength of the sintered body*

Simulating the sinter granulation process, 1.8~2.0 mm size fractions of iron ore were slightly shattered, and the pre-sintered hematite reagents with 15 wt pct CaO reagents were adopted as nuclei particles and adhering fines, respectively. The quasi-particle samples were granulated by laboratory pelletizer. As shown in Figure 3, the dried quasi-particles were fed into a quartz crucible (Φ16 × 20 mm), and the micro-sintering test was conducted with the same system as Figure 2(b). The sintered body was dropped down from a 2 m height to steel plate (H = 20 mm, S = 2.25 m^2) 10 times. Then, the bonding strength (abbreviated to BS) could be calculated according to Eq. [2].

$$\text{BS} = \frac{M_{+5\,\text{mm}}}{M} \times 100\ \text{pct}, \quad [2]$$

where $M_{+5\ \text{mm}}$ is the mass of the particles over 5 mm after dropped down 10 times, g. M is the mass of the sintered body, g.

III. RESULTS AND DISCUSSION

A. *Melt Absorbability of Iron Ore and Microstructure Feature of Sintered Tablets*

Microstructure mineralography images of cross sections after the melt absorbability tests are shown in

Table I. Chemical Composition and Major Mineral Type of Iron Ores

Iron Ore	Chemical Composition/Wt Pct							Main Iron-Bearing Mineral Constitute
	TFe	FeO	SiO_2	CaO	Al_2O_3	MgO	LOI	
OA	57.31	0.53	6.11	0.11	1.45	0.35	10.72	Goethite
OB	58.31	0.17	4.10	0.10	1.53	0.31	10.97	Goethite
OC	62.13	0.21	3.77	0.11	1.87	0.33	5.69	Goethite and Hematite
OD	61.49	0.28	4.74	0.06	2.48	0.35	4.80	Goethite and Hematite
OE	64.87	0.15	1.93	0.11	1.39	0.12	3.05	Hematite
OF	63.28	0.21	5.83	0.10	1.05	0.79	2.19	Hematite

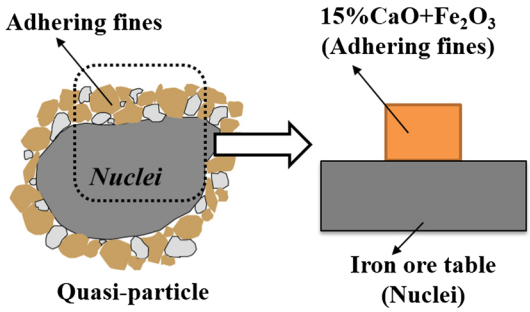

Fig. 1—Schematic diagram of coupled ore tablets simulating quasi-particle structure.

Figure 4(a). The red dotted line is the penetration limit of the secondary melts, and the blue solid line represents the initial reaction interface. Figure 4(b) shows the measurement results for penetration length. Limonite OA and OB have larger penetration depths, approximately 1.4 mm, and there were many large pores inside the melts. The penetration depths of OE and OF were smaller at, only approximately 0.4 mm. The melt absorbability of the nuclei ore can be expressed as penetration depth, which means that limonite ore has stronger melt absorbability, indicating that it has intense assimilation reactions with adhering fines. In contrast, the dense hematite ore has less melt absorbability.

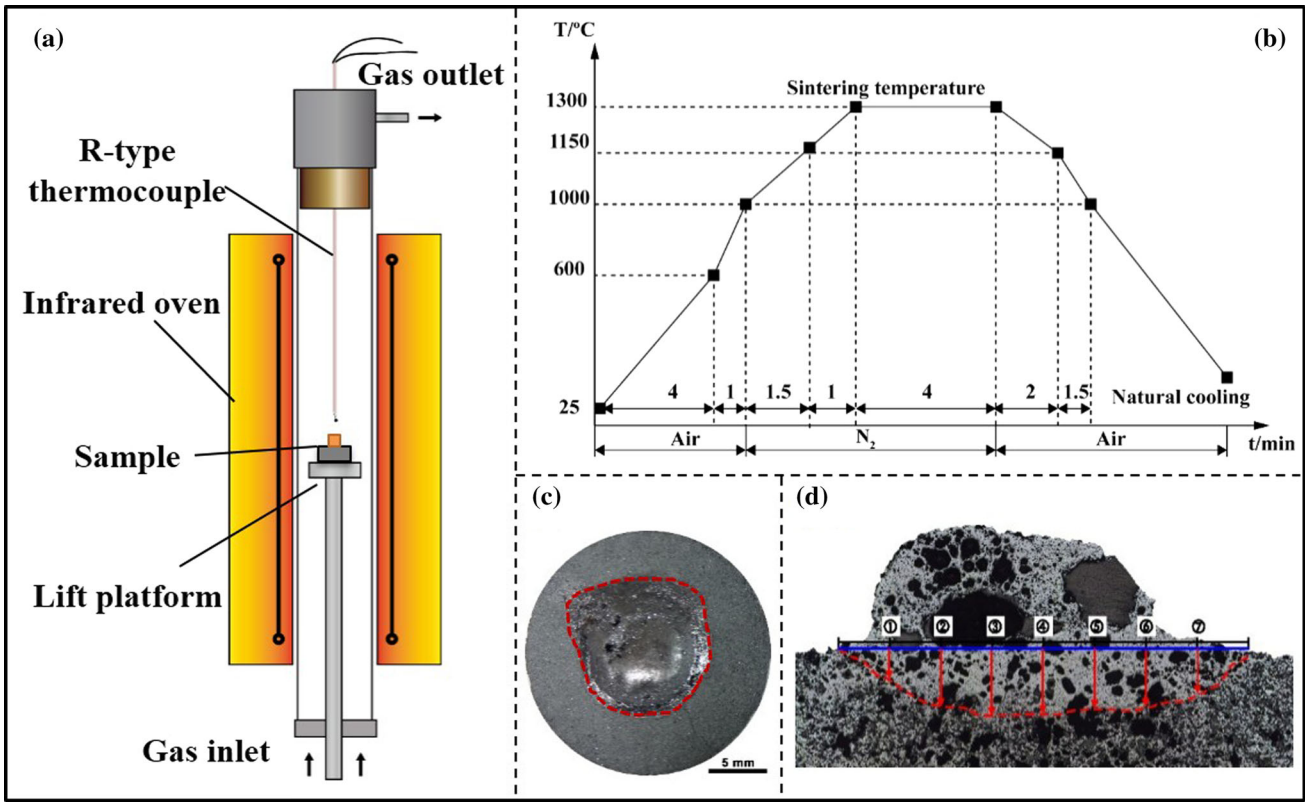

Fig. 2—Experimental condition and schematic diagram of melt absorbability and fluidity test. (*a*) Micro-sintering apparatus (*b*) experimental temperature and atmosphere system (*c*) flow area of effective liquid phase (*d*) measuring positions of melt penetration depth.

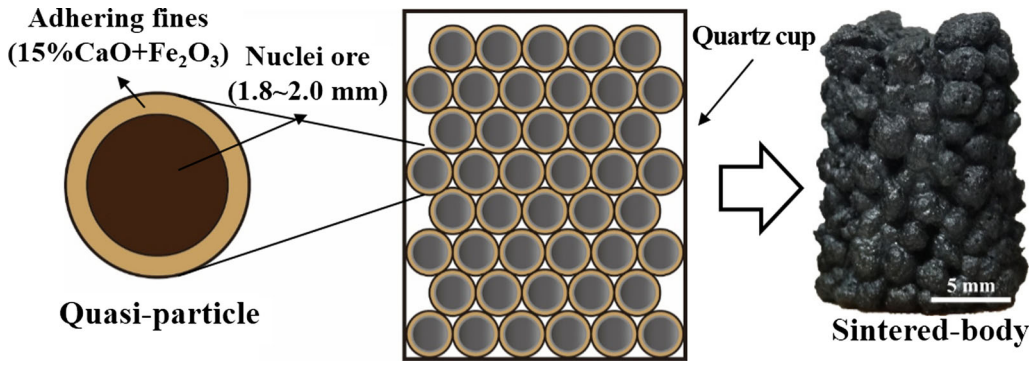

Fig. 3—Schematic diagram of bonding strength test.

The microstructural features of the coupled ore tablets were analyzed using an optical microscope. In general, taking OA as an example, it could be divided into three representative zones: the primary melt zone, the secondary melt zone, and the original ore zone. As shown in Figure 5(a), the main minerals in the primary melt zone included plenty of calcium ferrite (abbreviated to CFx) with some hematite; the central region had dissolved textures of CFx locally with fine magnetite or martite grains. In the upper portion of the secondary melt zone, the main minerals were silicoferrite of calcium and aluminum (abbreviated to SFCA) and hematite (Figure 5(b)). Nearby the leading edge line, it transformed into a structure of silicate minerals filled with hematite grains ultimately because the CaO content of penetration melts reduced drastically with assimilation between primary melts and nuclei ore proceeding continuously,[19] as shown in Figures 5(c) and (d).

B. *Factors that Influence Melt Absorbability and Reaction Behaviors of Secondary Melts*

In this study, analytically pure chemical reagents were used to study the effects of iron mineral type and gangue content on melt absorbability. The assimilation reaction behaviors of secondary melts were also discussed.

1. *Influence of iron mineral type on melt absorbability*

The major iron mineral types commonly used in sintering are hematite, limonite (goethite), and magnetite. Therefore, the pre-sintered Fe_2O_3 reagent, $Fe(OH)_3$, and Fe_3O_4 reagents were ground into fines with diameters less than 0.074 mm to simulate the above minerals. The microstructure mineralography and the melt penetration depth results are compared in Figure 6.

It can be seen from Figure 6 that the penetration depth of the goethite substrate is largest, followed by hematite and then magnetite. These results might be explained by the crystal water decomposition of goethite during the heating process from 473 K (200 °C) to 673 K (400 °C), which provided melt permeation channels by forming a loose porous structure and simultaneously promoted the kinetics of the assimilation reaction between the primary melt and nuclei particles as the specific surface area increased.[20] In the case of the magnetite substrate, because Fe_3O_4 cannot react with CaO directly, the inner section was not oxidized adequately, which prevented further diffusion of Ca^{2+}, thus reducing the penetration behavior of the primary melts. Figure 7 shows the relationship between the lowest assimilation temperature (abbreviated to LAT) and the melt penetration depth of the iron ore sample. It is found that the melt penetration depth decreases with the increase in LAT. This decrease occurs because the primary melts need a higher temperature to react with nuclei particles to generate secondary melts due to the weakening of assimilation. Additionally, under the condition of a fixed sintering temperature, the superheat degree of the formed secondary melt is diminished as LAT increases, and then the fluidity is suppressed which lead to a decrease in the melt penetration depth.

2. *Influence of gangue content on melt absorbability and reaction behaviors*

Referring to the actual chemical composition of iron ore, analytical grade Fe_2O_3 reagents with different proportions of SiO_2 or Al_2O_3 were used to simulate different gangue content ores (shown in Table II). Each group of mixtures was homogenized by grinding in anhydrous ethanol for approximately 20 minutes using an agate mortar. To better simulate natural ore, these chemical agent mixtures were pre-sintered at 1473 K (1200 °C) for 480 minutes in a muffle furnace. Then, the pre-sintered samples were crushed into particles with diameters less than 0.074 mm. The melt absorbability test was employed to measure the melt penetration depth of each sample. SEM and EDS analyses were conducted to examine the influence of gangue content on melt penetration reaction behaviors.

Figures 8 and 9 show the BSE images and EDS analysis results of melt penetration zone (A) and (B) in S-4 and A-4 samples, respectively. From the EDS analysis results, it is concluded that the melts are calcium ferrite containing SiO_2 or Al_2O_3 in the melt penetration center area (A). At the front edge of the melt penetration zone (B), the Si element is enriched, and the minerals formed by the enrichment are mainly silicate. However, for different Al_2O_3 content substrates, enriched calcium aluminate is not found. Other samples demonstrate similar reaction behaviors for secondary melts.

It can be concluded that there are different reaction behaviors in the melt penetration process into SiO_2 or Al_2O_3 containing substrates.

The melt penetration reaction behavior mechanism for SiO_2 containing substrates is summarized as follows:

(a) A calcium ferrite melt initially forms in the region of the adhering fines by a reaction of hematite with CaO.

$$Fe_2O_3 + CaO = CaO \cdot Fe_2O_3$$

(b) Assimilation starts with the penetration of the calcium ferrite melt into the nuclei that reacts with nuclei compositions (Fe_2O_3, SiO_2) to form a new melt SFC through major substitutions among Ca^{2+}, Si^{4+}, and Fe^{3+} ions ($2(Fe^{3+}) = Ca^{2+} + Si^{4+}$)[21,22]

$$SiO_2 + CaO \cdot Fe_2O_3 + Fe_2O_3 = SFC$$

(c) During penetration, the viscosity of the melt gradually increases as SiO2 and Fe_2O_3 of the nuclei dissolved into the melt. As amount of SiO_2 solution increases, the SFC melts are broken down. On the other hand, the partially high SiO_2 concentration leads to the formation of silicate minerals (such as $3CaO{\cdot}Fe_2O_3{\cdot}3SiO_2$)[23]

$$SiO_2 + SFC \rightarrow CaO \cdot SiO_2 + Fe_2O_3$$

$$3SiO_2 + 3CaO + Fe_2O_3 = 3CaO \cdot Fe_2O_3 \cdot 3SiO_2$$

(d) Finally, granular hematite and silicate phases are precipitated upon cooling in the leading edge of melts penetration.

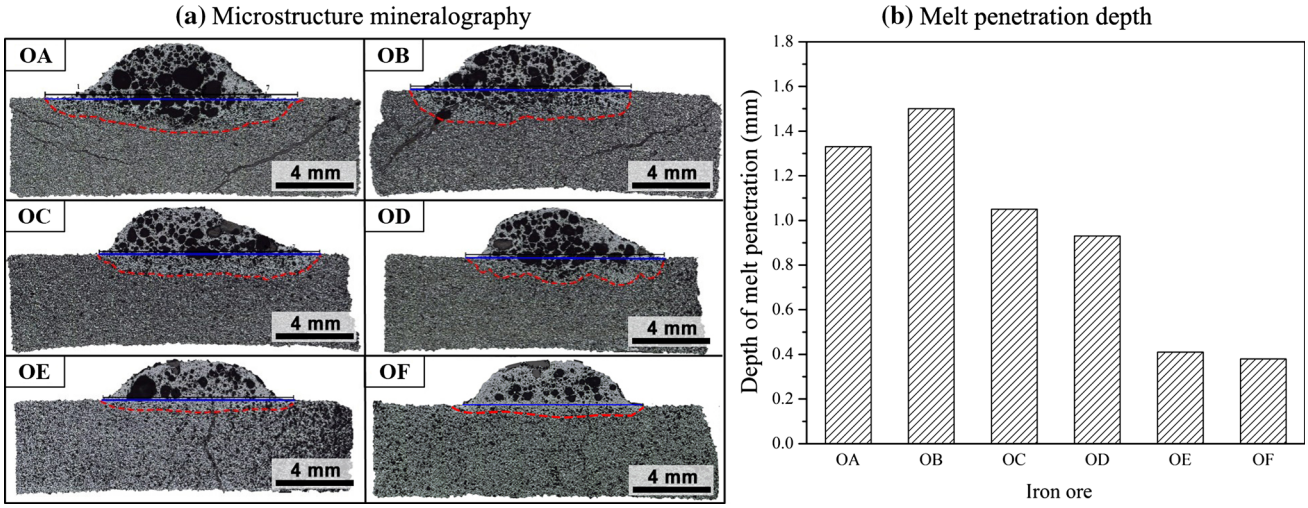

Fig. 4—Microstructure mineralography and melt penetration depth of different iron ore samples. (*a*) Microstructure mineralography (*b*) Melt penetration depth.

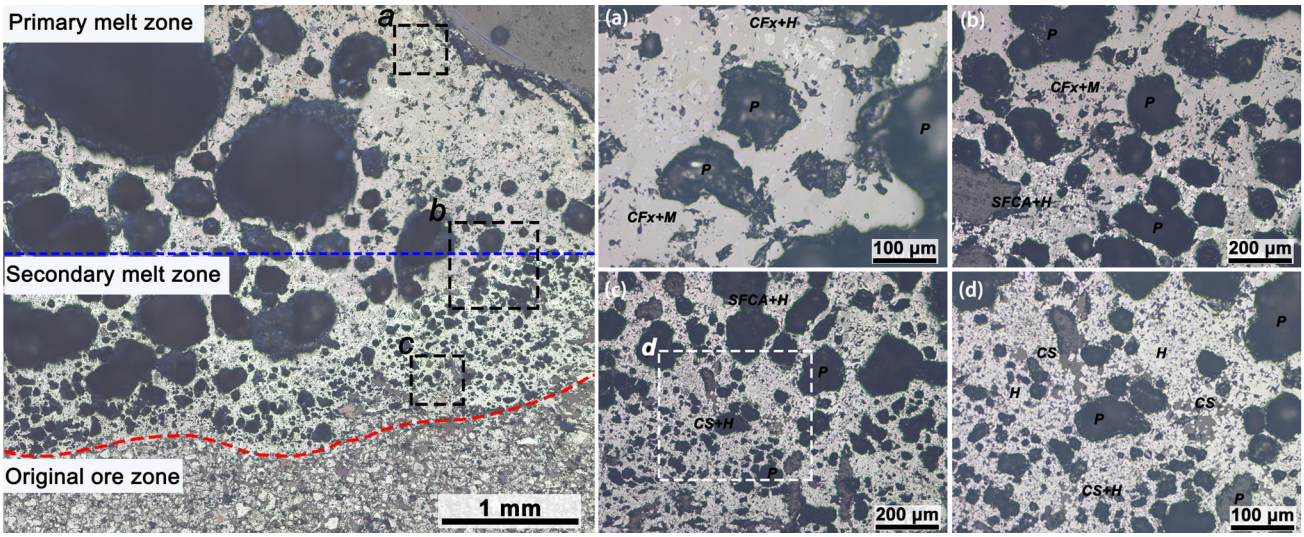

Fig. 5—Microstructural features of the OA sample. (*a*) Primary melt zone (*b*) Transition melt zone (*c*) Secondary melt zone (*d*) Typical structure of silicate minerals filled with hematite in secondary melt zone.

This change in mineral structure is consistent with the observation of natural iron ore substrates.

Lister *et al.*[24] found that CaO·3(Al2O3, Fe2O3), defined as the "ternary phase" (TP), appeared in the Fe2O3-CaO-Al2O3 system and was stable between 973 K (700 °C) and 1723 K (1450 °C). The melt penetration reaction behavior mechanism for Al_2O_3 containing substrates is as follows:

$$CaO \cdot Fe_2O_3 + Fe_2O_3 + Al_2O_3 \rightarrow TP$$

The melt penetration depth results for different SiO_2 or Al_2O_3 content substrates are presented in Figure 10. The melt penetration depth decreases as the gangue content increases when the content of SiO_2 or Al_2O_3 is less than 5 wt pct, and the degree of decrease in the Al_2O_3-containing substrates is slightly larger than that of the SiO_2-containing substrates. The penetration behavior is essentially determined by the melt properties in terms of the ratio of surface tension to viscous force (i.e., $\gamma \cos\theta/\eta$), and there has been some research indicating that the penetration depth of calcium ferrite melts is believed to be dominantly affected by the melt viscosity.[1,14,25–27]

When the SiO_2 content exceeds 6 wt pct, the reduction in melt penetration depth decreases. It is thought that many silicate melts (3CaO·Fe2O3·3SiO2) are formed after the primary melt reacted with high SiO_2 content substrates because Ding *et al.*[23] found that the solid solution limit content of SiO_2 is 5.21 to 6.11 wt pct in SFC. Therefore, the amount of SFC in lower melting point materials is reduced. Finally, a dramatic increase in melt viscosity and a serious deterioration in the fluidity make it difficult for silicate melt to continually penetrate down.

In summary, the most important factor influencing melt absorbability is iron mineral type, and limonite has

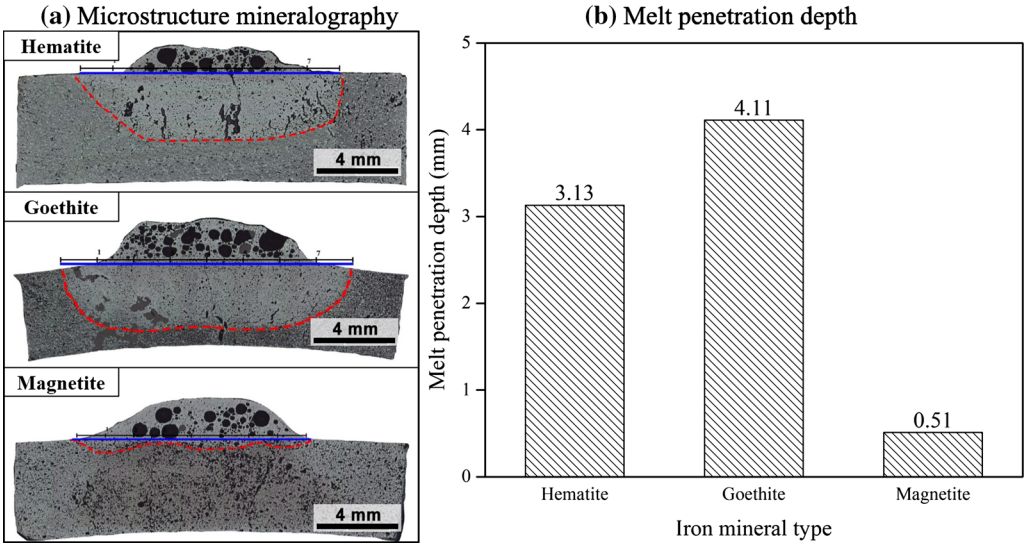

Fig. 6—Microstructure mineralography images and melt penetration depth of different iron minerals. (*a*) Microstructure mineralography (*b*) Melt penetration depth.

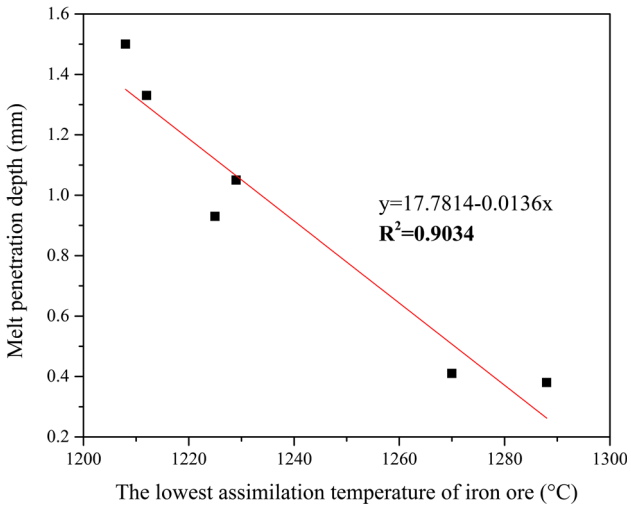

Fig. 7—Relation between the lowest assimilation temperature and the melt penetration depth.

higher melt absorbability than hematite and magnetite. Then, the gangue composition, either SiO_2 or Al_2O_3 in nuclei ores, inhibits melt penetration depth, and the impact of Al_2O_3 content is larger.

C. *Influence of Melt Absorbability on the Bonding Strength of the Sintered Body*

The primary melts formed by adhering fines reacted with nuclei particles to generate secondary melts in the sintering process. The generating capacity of secondary melts and the quality of the bonding phase were largely determined by the melt absorbability of the nuclei, which affected the bonding strength of the sintered body.

To investigate the effect of melt absorbability on effective liquid phase fluidity and the bonding strength of the sintered body, the fluidity index of the effective liquid phase on the six iron ore substrates and the bonding strength of the sintered bodies that consist of these different nuclei particles were measured, respectively. The effective liquid phase fluidity was defined as the increase of vertical projection area after the melt flowed on the surface of the different iron ore substrates, which calculated according to Eq. [1]. The fluidity of primary melts was measured on a dense inert alloy plate, which can avoid the influence of melt absorbability. According to the bonding strength of the sintered body test, the 1.8 to 2.0 mm of six iron ore particles were conducted as nuclei, respectively, and the mixture of pre-sintered hematite (crushed into less than 0.074 mm) and 15 wt pct CaO reagent were adhering fines. The ratio of nuclei particles to adhering fines was fixed at 7:3 for each sample. The granulated samples were sintered at 1573 K (1300 °C), and then the bonding strengths of these sintered bodies were measured.

The relationship between the melt penetration depth and fluidity of the effective liquid phase is presented in Figure 11(a). It shows a negative correlation between these variables. The reduction in the fluidity of the effective liquid phase might be caused by the decrease in the liquid content, which results from the primary melt

Table II. Chemical Composition of Different SiO_2 or Al_2O_3 Containing Substrates (Wt Pct)

Sample	Fe_2O_3	SiO_2	Al_2O_3
S-2	98.0	2.0	—
S-4	96.0	4.0	—
S-6	94.0	6.0	—
S-8	92.0	8.0	—
S-10	90.0	10.0	—
A-1	99.0	—	1.0
A-2	98.0	—	2.0
A-3	97.0	—	3.0
A-4	96.0	—	4.0
A-5	95.0	—	5.0

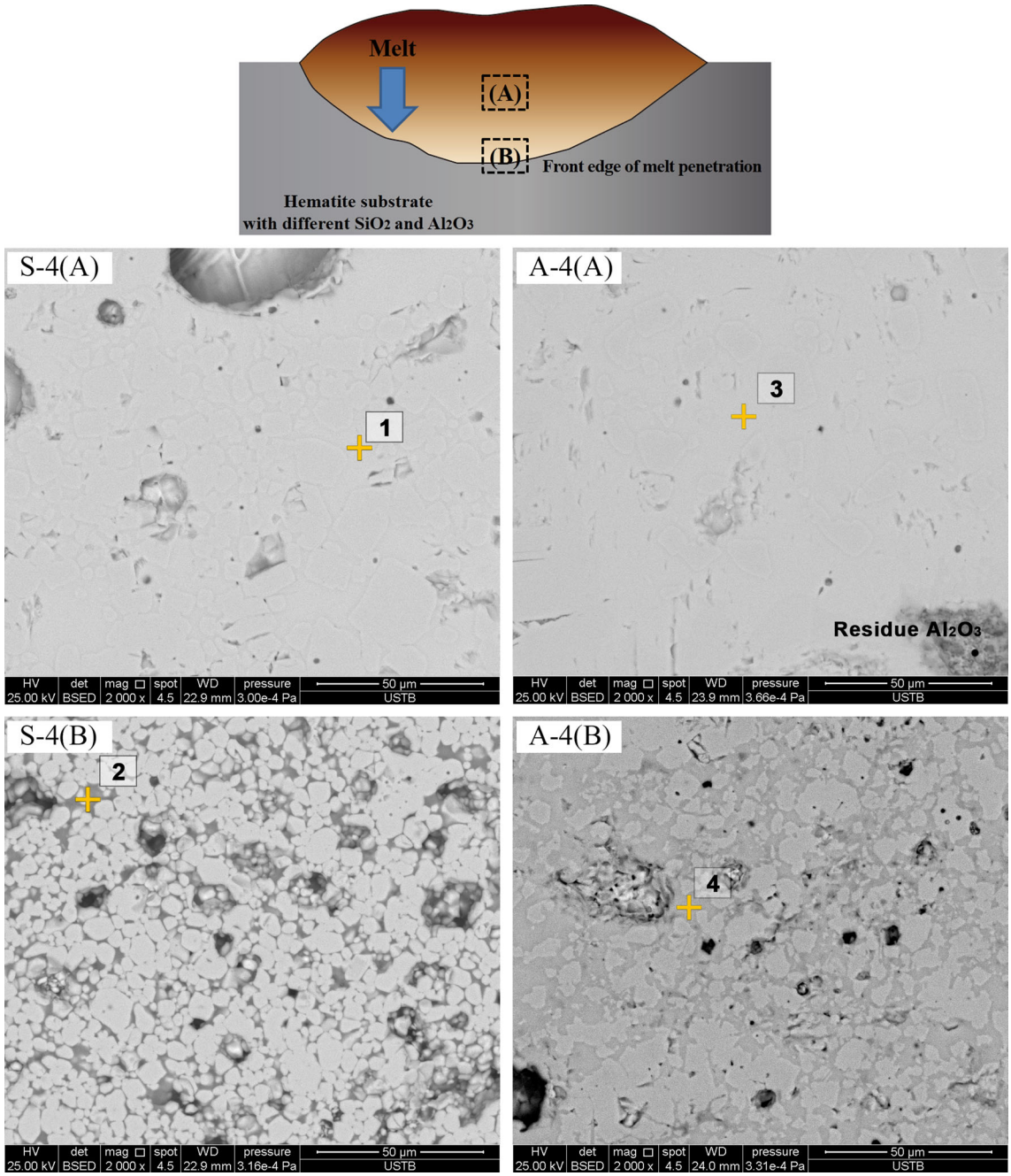

Fig. 8—BSE image of melt penetration zones A and B in S-4 and A-4 samples, respectively.

penetrating into nuclei particles. On the other hand, the viscosity of the effective liquid boundary layer increased due to the diffusion of gangue composition. The contact angle of the effective liquid phase became larger, and the wetting ability is weakened, which makes fluidity of the effective liquid decline. Figure 11(b) shows the relation between the melt penetration depth and the bonding strength of the sintered body. The figure also shows a negative linear relationship. The reason is that nuclei particles with high melt absorbability lessen the quantity of effective liquid, and simultaneously, the fluidity of the secondary melt decreases due to the melt penetration reaction. Both of these factors weaken the effective bonding between quasi-particles. The relationship between the bonding strength of the sintered body and the fluidity of the effective liquid phase is shown in Figure 12. Consequently, the nuclei particles with stronger melt absorbability are not conducive to improving the bonding strength of the sintered body.

The sinter quasi-particle is composed of nuclei and high basicity adhering fines, and the sintered body is made of bonded quasi-particles. Thus, the bonding strength of the sintered body is mainly affected by the following factors. The first factor is the bonding ability of the primary melts generated by adhering fines, which could be characterized by the liquid phase fluidity of the

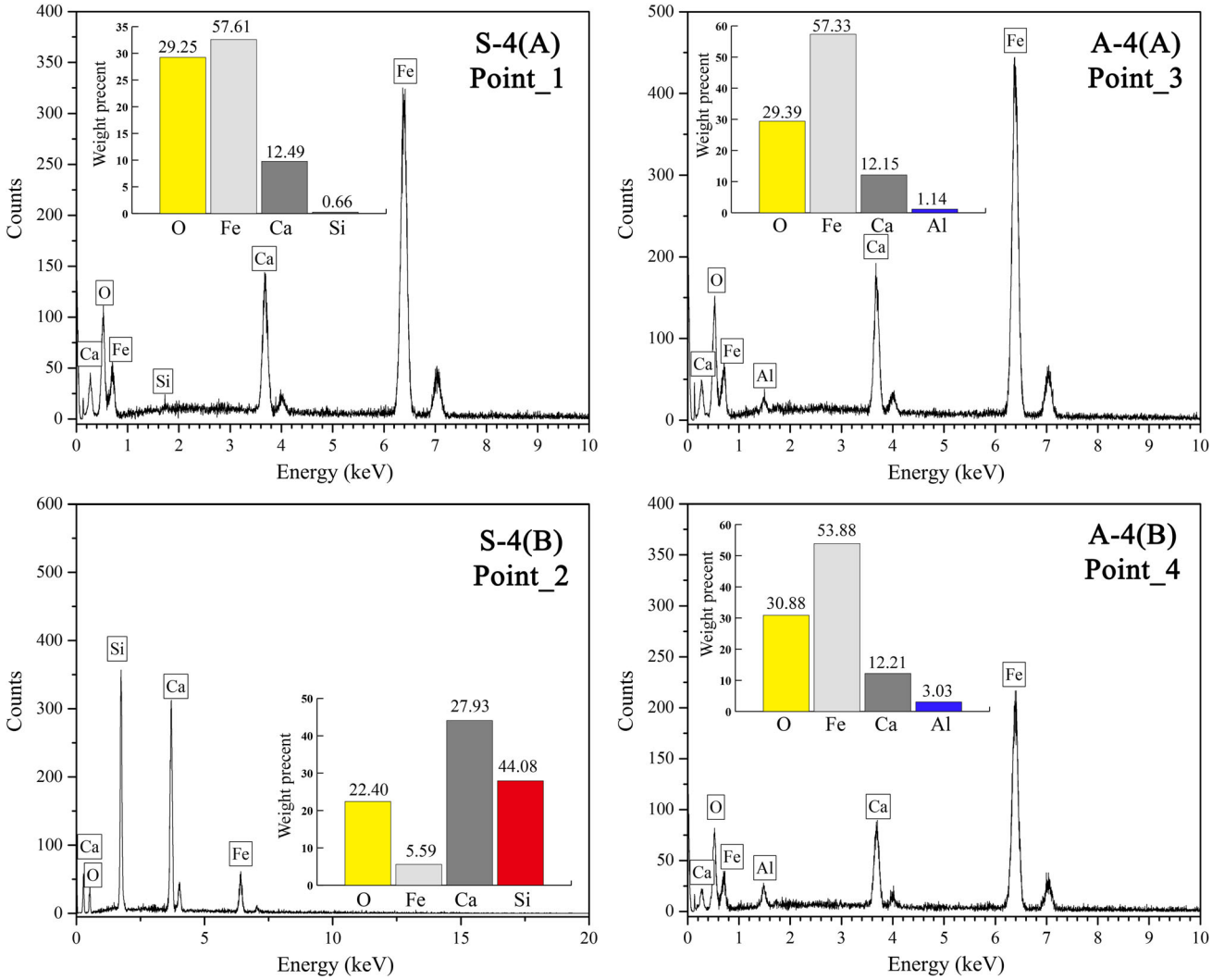

Fig. 9—EDS analysis results of melt penetration zones A and B in S-4 and A-4 samples, respectively.

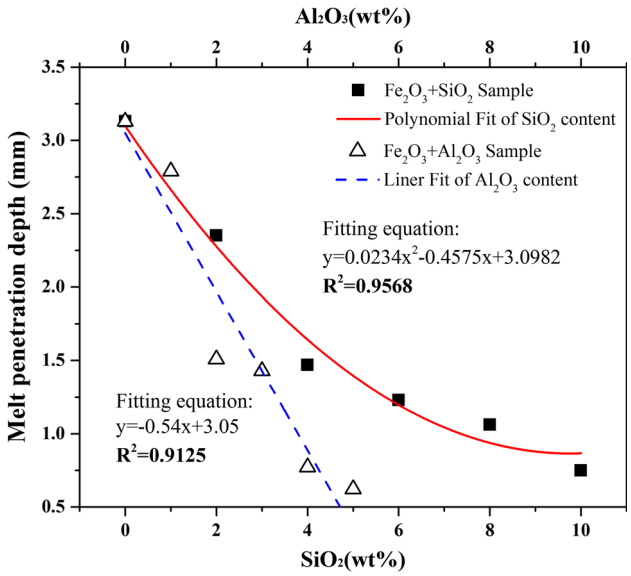

Fig. 10—Melt penetration depth of different SiO_2 or Al_2O_3 content substrates.

adhering fines. The second factor is the weakening effect of the melt absorbability of nuclei particles on the fluidity of primary melts, which is mainly due to the assimilation reaction of nuclei particles with primary melts.

Therefore, the bonding strength (BS) of the sintered body can be expressed by Eq. [3].

$$BS_{(Sintered\ body)} = BS_{(Primary\ melt\ fluidity)} - BS_{(Nuclei\ assimilability)} \quad [3]$$

According to the fitted formulas for melt penetration depth with bonding strength (as Figure 10(b)), liquid phase fluidity with bonding strength (as Figure 11), and melt penetration depth with the lowest assimilation temperature (as Figure 7), the bonding strength (BS) model can be represented as a function of liquid phase fluidity (LPF) of adhering fines and the lowest assimilation temperature (LAT) of nuclei particles as follows:

$$BS_{(Sintered\ body)} = (51.02LPF - 15.523) - 22.70 \times (17.7814 - 0.0136LAT) \quad [4]$$

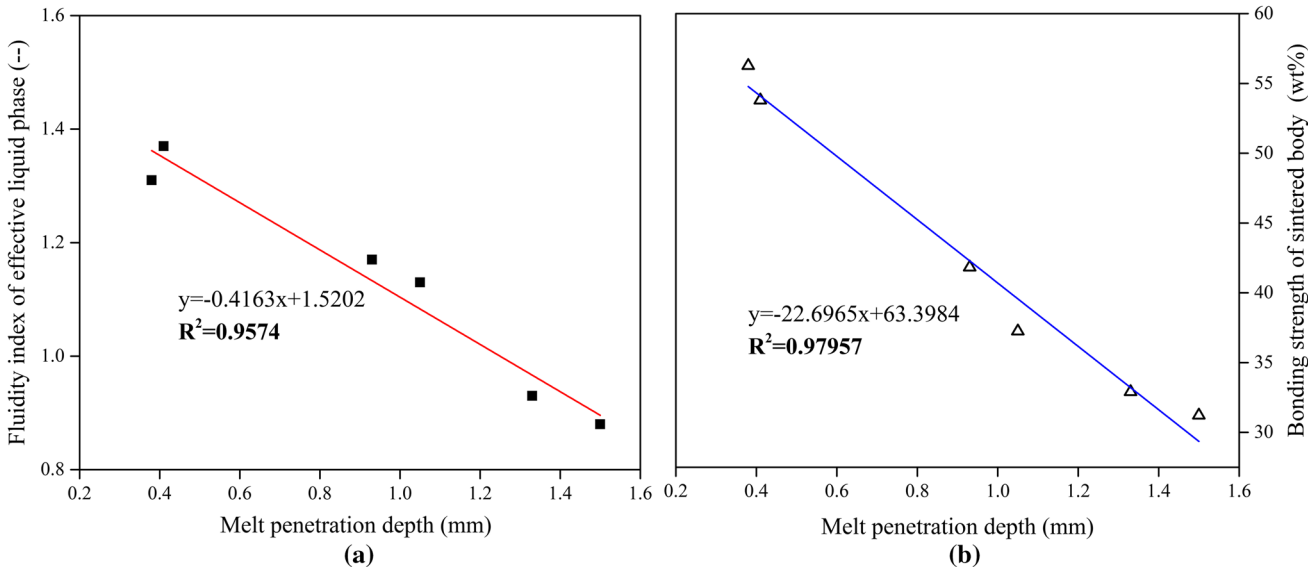

Fig. 11—Relationship between the melt penetration depth and (*a*) Fluidity index of the secondary liquid phase (*b*) Bonding strength of the sintered body.

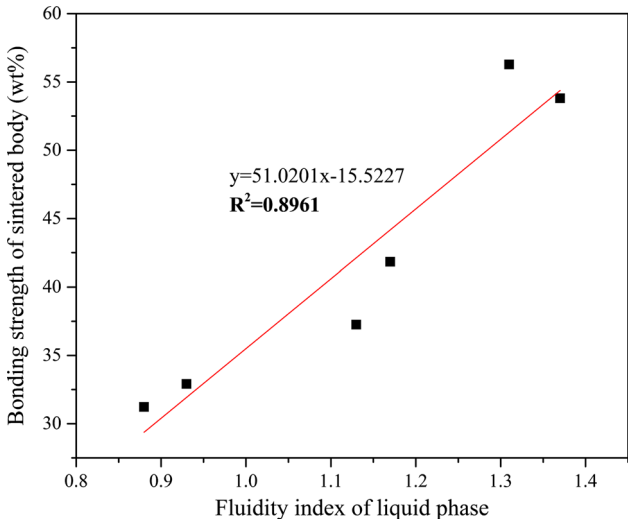

Fig. 12—Relationship between the fluidity index of the effective liquid phase and the bonding strength of the sintered body.

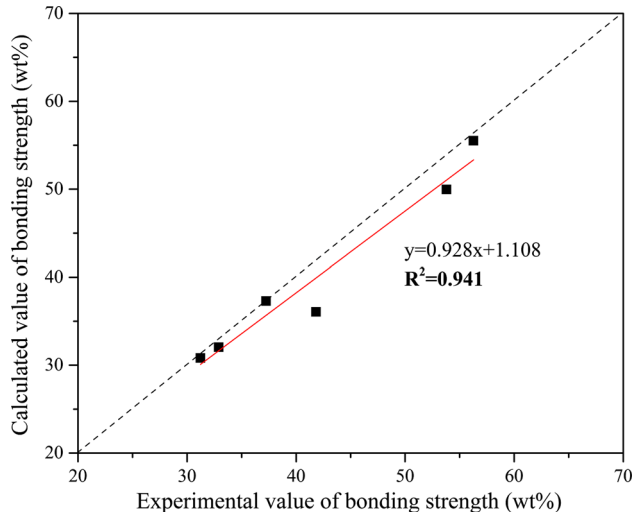

Fig. 13—Relationship between the calculated and experimental $BS_{(sintered\ body)}$ values.

In general, the actual sintering temperature is approximately 1573 K (1300 °C),[28] and the difference between the sintering temperature and the lowest assimilation temperature of iron ore is defined as the drive temperature of melt absorbability (ΔT_{LA}), which represents the superheat of the assimilation reaction (melt absorption process) of the nuclei particles. The greater the ΔT_{LA}, the earlier the melt absorption reaction occurs during the sintering process. Bringing in Eq. [4], it can be simplified as Eq. [5].

$$BS_{(Sintered\ body)} = 51.02LPF - 0.30872\,(\Delta T_{LA}) - 17.825\,(LPF \geq 0.35) \quad [5]$$

The bonding strength values of the sintered body were calculated based on the fluidity index of the primary melt and the lowest assimilation temperature of the different iron ores that were measured previously. Figure 13 shows the comparison between calculated and experimental $BS_{(sintered\ body)}$ values. The calculated values are close to the measured ones. This result might indicate that the bonding strength of the sintered body can be characterized and predicted by the fluidity of primary melts and the assimilability of nuclei to some extent. According to the above formula, to improve the bonding strength of the sintered body, we should improve the liquid phase generation capacity of adhering fines, enhance its fluidity, or reduce the drive temperature of melt absorbability (ΔT_{LA}) through optimizing the ore blend structure or the proper design of quasi-particles, thereby inhibiting melt absorption of nuclei particles. Furthermore, the liquid fluidity index

should remain at least 0.35 so that the effective bonding can be produced between the quasi-particles, even though melt absorbability can be ignored in some cases.

D. *Suitable Liquid Contents of the Sintered Body for Different Melt Absorbability Iron Ores*

To investigate the effect of melt absorbability of iron ores on the suitable liquid content of the sintered body, two typical melt absorbability nuclei particles (OB and OF) were selected to measure the bonding strengths of the sintered bodies under different ratios of nuclei to adhering fines. The specific experimental procedure was described in Section II–B, and the results are shown in Figure 14. The bonding strengths of each sintered body rise with the increase in the proportion of adhering fines. This increase is because the increased adhering fines enhanced the amount of effective liquid phase. In addition, since the thickness of the adhering fines layer increases, the impact of the melt absorbability of nuclei ore on the outer layer of adhering fines is also weakened, which improves the liquid fluidity of the outer layer and enhances the bonding effect of the quasi-particles. Referring to the practical sintering yield indicators, the bonding strength at the 75 pct level is defined as the qualified line and is presented in Figure 14. With the strong melt absorbability ore OB as nuclei particles, the ratio of adhering fines required to reach the qualified product is 39.12 pct, while that of ore OF as nuclei particles is 35.83 wt pct. The amount of liquid phase which adhering fines generated is calculated by FactSage 7.0 software. Combined with the proportion of adhering fines, the suitable liquid contents of the sintered body OB and OF samples are 31.36 and 28.56 pct, respectively. Consequently, for the quasi-particles, the iron ore nuclei particles have different melt absorbability the required amount of primary melt is not same. To meet the requirements for the bonding strength of the sintered body, high melt absorbability nuclei need adhering fines to provide more primary melts.

Since blast furnace ironmaking has relatively specific requirements for sinter basicity and SiO_2 content, the added proportion of calcium flux was essentially constant in practical sintering process. However, the adjustment of ore blend type, such as increasing the ratio of iron concentrate, will result in the changes to the ratios of nuclei to fines and the CaO content of adhering fines. The influence of nuclei/fines ratios on bonding strength with the constant addition of CaO to the quasi-particles was investigated to guide the optimization of ore blending and the design of the quasi-particles. Table III lists the experimental schemes, and the bonding strength results are presented in Figure 15.

It can be seen that under fixed CaO ratio conditions, with the increasing proportion of adhesive powder in quasi-particles, the CaO content in the adhering fine decreases gradually, and the bonding strength of the

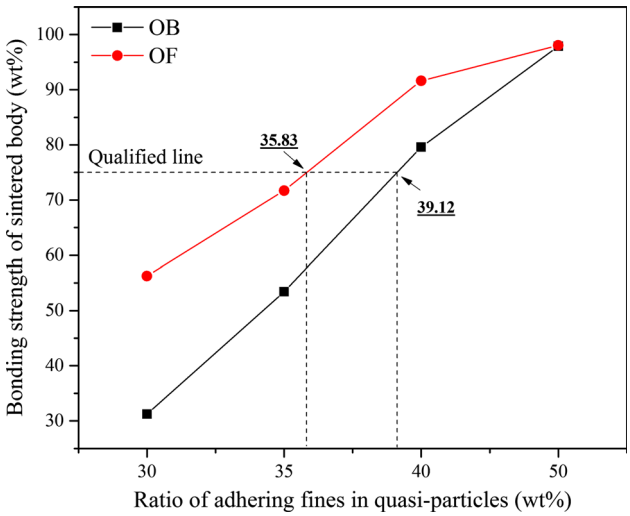

Fig. 14—Bonding strengths of sintered bodies with different adhering fines ratios in quasi-particles.

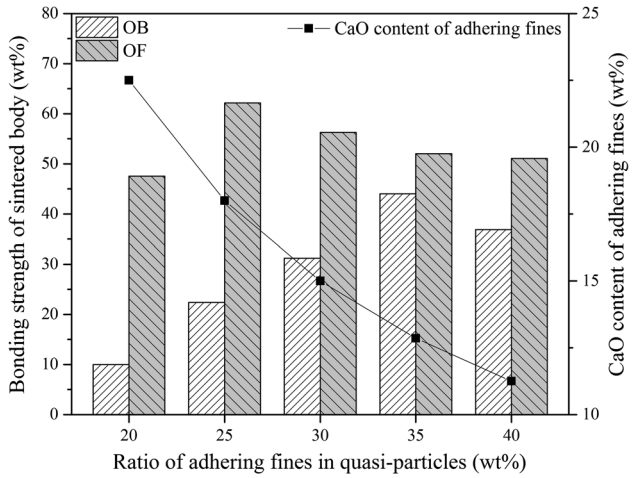

Fig. 15—The bonding strengths of sintered bodies with different adhering fines ratios with the condition of fixed CaO content.

Table III. Bonding Strength Test Scheme in Fixed CaO Content

Ratio of Nuclei/Adhering Fins (Wt Pct)		CaO Content (Wt Pct)	
Nuclei Particles	Adhering Fines	In Sintered Body	In Adhering Fines
80	20	4.50	22.50
75	25	4.50	18.00
70	30	4.50	15.00
65	35	4.50	12.86
60	40	4.50	11.25

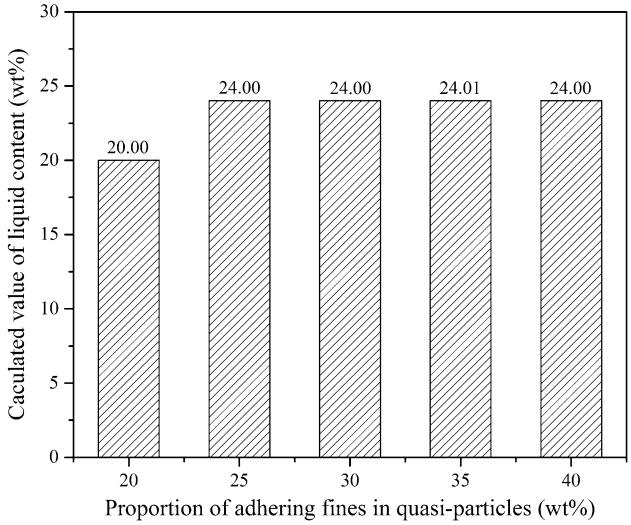

Fig. 16—The calculation of liquid content in sintered bodies with different adhering fines ratios under the fixed CaO content condition.

sintered body increases first and then decreases. OB nuclei sample grains the maximum at the adhering fines ratio is 35 wt pct, compared to 25 wt pct for OF nuclei samples.

The primary melt contents of each sintered body were also calculated by FactSage7.0, as shown in Figure 16. The liquid contents are the same after the adhering fines ratio reaches 25 wt pct or more. This result suggests that with the same liquid content, an appropriate increase in the ratio of adhering fines and decrease in segregation basicity (or CaO content) are beneficial to improving the bonding strength of the sintered body for stronger melt absorbability nuclei ore. This result might be ascribed to the influence of the CaO concentration gradient on melt absorption behavior. A higher CaO concentration gradient enhances the assimilation reaction of the primary melt and nuclei particles, but this finding may need further investigation. On the other hand, the direction is just the opposite for weaker melt absorbability nuclei ore, which is due to the reduced effect of melt absorbability of nuclei particles on primary melts, such that the fluidity of the effective liquid phase could be improved as the basicity of adhering fines increased. Therefore, the bonding strength is enhanced due to the promotion of adhesion between quasi-particles.

IV. CONCLUSIONS

To clarify the important effect of nuclei ore properties on the bonding strength and suitable liquid content of the sintered body, micro-sintering melt absorbability and bonding strength tests were conducted. The main factors influencing melt absorbability, the assimilation reaction behavior of the primary melt into nuclei, and the influence of the nuclei/adhering fines ratio on bonding strength were also discussed. The following conclusions were drawn.

(1) The melt absorbability of iron ore has a negative correlation with the lowest assimilation temperature, such that the assimilation thermodynamic conditions could be considered the major driving force of the melt penetration behavior of the primary melt into the nuclei ore.
(2) The most important mineralogy factor influencing melt absorbability is iron mineral type. The melt absorption degree of goethite is largest, followed by hematite, and magnetite. Then, the gangue composition, either SiO_2 or Al_2O_3, in nuclei ores inhibited melt penetration depth, and the impact of Al_2O_3 content is larger.
(3) The penetration behaviors of melts into SiO_2 or Al_2O_3 containing substrates are different. In the penetration process, SiO_2 and Al_2O_3 dissolve into melts to form ferrite, as SFC or TP. With the increasing concentration of SiO_2 or Al_2O_3 in melts, SFC is decomposed into silicate ($3CaO{\cdot}Fe_2O_3{\cdot}3SiO_2$), especially if the SiO_2 content exceeds 6 wt pct, which is consistent with TP melts for Al_2O_3 containing substrates.
(4) The bonding strength of the sintered body is collectively determined by the liquid phase fluidity of adhering fines and the assimilability of nuclei ore, which could be expressed by the formula $BS_{(Sinteredbody)} = 51.02LPF - 0.30872(\Delta T_{LA}) - 17.825$. The stronger the melt absorbability of the nuclei ore, the lower the bonding strength of the sintered body.
(5) To meet the requirements for the bonding strength of the sintered body, the required amount of primary melt is not the same for different melt absorbability nuclei ore. The high melt absorbability nuclei need adhering fines to provide more primary melts. Furthermore, in the condition of the same liquid content, for stronger melt absorbability nuclei ore, an appropriate increase in the adhering fines ratio and reduction in the segregation basicity are more conducive to improving the bonding strength.

REFERENCES

1. N. Oyama, T. Higuchi, S. Machida, H. Sato, and K. Takeda: *ISIJ Int.*, 2009, vol. 49, pp. 650–58.
2. T. Otomo, Y. Takasaki, and T. Kawaguchi: *ISIJ Int.*, 2005, vol. 45, pp. 532–37.
3. J.W. Jeon, S.W. Kim, and S.M. Jung: *ISIJ Int.*, 2015, vol. 55, pp. 513–20.
4. E. Kasai and F. Saito: *ISIJ Int.*, 1996, vol. 36, pp. 1109–11.
5. S.L. Wu, Y. Liu, and J. Du: *J. Univ. Sci. Technol.*, 2002, vol. 24 (3), pp. 254–57.
6. G. Zhang, S.L. Wu, B. Su, Z.G. Que, C.G. Hou, and Y. Jiang: *Int. J. Miner. Metall. Mater.*, 2015, vol. 22, pp. 553–61.
7. N. Scarlett, M.I. Pownceby, I.C. Madsen, and A.N. Christensen: *Metall. Mater. Trans. B*, 2004, vol. 35B, pp. 929–36.
8. B. Yu, X.W. Lv, S.L. Xiang, and J. Xu: *Metall. Mater. Trans. B*, 2016, vol. 47B, pp. 2063–71.
9. B. Yu, X.W. Lv, S.L. Xiang, C.G. Bai, and J.Q. Yin: *ISIJ Int.*, 2015, vol. 55, pp. 1558–64.
10. S.L. Xiang, X.W. Lv, B. Yu, J. Xu, and J.Q. Yin: *Metall. Mater. Trans. B*, 2014, vol. 45B, pp. 2106–17.

11. N. Saito, N. Hori, K. Nakashima, and K. Mori: *Metall. Mater. Trans. B*, 2003, vol. 34B, pp. 509–16.
12. J. Peng, L. Zhang, L.X. Liu, and S.L. An: *Metall. Mater. Trans. B*, 2017, vol. 48B, pp. 538–44.
13. H.M. Long, X.J. Wu, T.J. Chun, Z.X. Di, and B. Yu: *Metall. Mater. Trans. B*, 2016, vol. 47B, pp. 2830–36.
14. J. Okazaki, K. Higuchi, Y. Hosotani, and K. Shinagawa: *ISIJ Int.*, 2003, vol. 43, pp. 1384–92.
15. S.L. Wu, B. Su, T.K. Song and X.B. Zhai: *Proceedings of the 10th CSM Steel Congress & the 6th Baosteel Biennial Academic Conference*. Metallurgical Industry Press, Beijing, Oct 2015, pp. 127-40.
16. S.L. Wu and G.L. Zhang: *Steel Res. Int.*, 2015, vol. 86, pp. 1014–21.
17. J. Zhu, S.L. Wu, J.X. Fan, G.L. Zhang, and Z.G. Que: *ISIJ Int.*, 2013, vol. 53, pp. 1529–37.
18. L. Xiong, X.M. Mao and J. Li: *Proceedings of the 10th CSM Steel Congress & the 6th Baosteel Biennial Academic Conference*. Metallurgical Industry Press, Beijing, Oct 2015, pp. 369–76.
19. F. Matsuno and T. Harada: *Trans. ISIJ*, 1981, vol. 21, pp. 318–25.
20. S.L. Wu, G.L. Zhang, S.G. Chen, and B. Su: *ISIJ Int.*, 2014, vol. 54, pp. 582–88.
21. M.I. Pownceby and T. Patrick: *Eur. J. Mineral.*, 2000, vol. 12, pp. 455–68.
22. X. Ding and X.M. Guo: *Metall. Mater. Trans. B*, 2014, vol. 45B, pp. 1221–31.
23. X. Ding, X.M. Guo, C.Y. Ma, K. Tang, and Y.D. Zhao: *Metall. Mater. Trans. B*, 2015, vol. 46B, pp. 1146–53.
24. D.H. Lister and F.P. Glasser: *BRIT CERAM SOC TRANS*, 1967, vol. 66, pp. 293–305.
25. J. Jeon, S. Kim, I. Suh, and S. Jung: *ISIJ Int.*, 2014, vol. 54, pp. 2713–20.
26. S. Yoshimura, K. Kurosawa, Y. Gonda, S. Sukenaga, N. Saito, and K. Nakashima: *ISIJ Int.*, 2009, vol. 49, pp. 687–92.
27. T. Maeda, K. Nishioka, K. Nakashima, and M. Shimizu: *ISIJ Int.*, 2004, vol. 44, pp. 2046–51.
28. N. Oyama, Y. Iwami, T. Yamamoto, S. Machida, T. Higuchi, H. Sato, M. Sato, K. Takeda, Y. Watanabe, M. Shimizu, and K. Nishioka: *ISIJ Int.*, 2011, vol. 51, pp. 913–21.